TEXTURE ANALYSIS OF CYLINDRICAL CUP DURING DEEP-DRAWING PROCESS

Paulo Flores, Laurent Duchêne and Anne Marie Habraken

Mechanical and Civil Engineering Institute,
M&S Department, University of Liège
Chemin des Chevreuils 1, 4000 Liège, Belgium

ABSTRACT : This paper presents the simulation of a deep-drawing process using three different constitutive laws: strain rate space yield locus description with an isotropic hardening law, strain rate space yield locus description with a combined (isotropic and kinematic) hardening law, and stress space yield locus description with an isotropic hardening law. To take into consideration material anisotropy, the yield locus is computed from the crystallographic texture using Taylor's model, a dual plastic potential and combined hardening law taking into account the dislocations microstructures. The results obtained by these three constitutive laws are compared with experimental ones.

1. INTRODUCTION

The industrial requirements (aerospace, car manufacturing) of lighter parts with high mechanical resistance and, at the same time high geometrical accuracy, have motivated the study of metals such as high strength steel and aluminum alloys, and their appropriate forming process. Several problems have been detected during metal forming processes, like springback, wrinkles and earing behavior caused by material anisotropy. The idea is to have a constitutive model for plastic behavior able to predict those phenomena. The model presented in this paper takes into account two sources of material anisotropy, the crystallographic texture and the strain-path induced anisotropy.

The description of a texture based anisotropic yield locus has been proposed by MTM of K.U. Leuven. This team has developed texture models in strain rate and stress space (Van Bael [1994] and Winters [1996] respectively), which allow to describe initial yield locus. Their method is based on texture measurements by X-Ray diffraction avoiding the performance of several mechanical tests needed to identify the initial yield locus.

The hardening model proposed by Teodosiu and Hu [1995] allows to describe the strain-path induced anisotropy considering the influence of the deformation history represented by internal variables. Hoferlin [2001] incorporates this hardening law and a strain rate space description of the initial yield locus into the finite element code *Lagamine* developed by M&S department at University of Liège.

This hardening law in addition with an isotropic one and the texture-based yield locus description will be briefly introduced in section 2. Section 3 is focused on the description of the type of finite element used and the chosen formulation. The application is a deep-drawing process modeled in section 4 as follows: first using a strain rate space formulation and an isotropic hardening law, second using a strain rate space formulation with Teodosiu and Hu's hardening law and finally using a stress space formulation and an isotropic hardening law. The results will be compared with experimental measurement and conclusions are established in section 5.

Considering that the plastic strain rate $\underline{\dot{\varepsilon}}^P$ is classically assumed to be deviatoric and that only the deviatoric stress tensor $\underline{\hat{\sigma}}$ matters with regard to plastic deformation these deviatoric tensors have only five independent variables. In order to save storage and time these second order tensors are represented by first order vectors limited to five components such that $\dot{\varepsilon}^P_{ij}\dot{\varepsilon}^P_{ij}=\dot{e}^P_p\dot{e}^P_p$ and $\hat{\sigma}_{ij}\hat{\sigma}_{ij}=\hat{\sigma}_p\hat{\sigma}_p$ with $i,j=1,\ldots,3$ and $p=1,\ldots,5$.

2. CONSTITUTIVE MODEL

To compute the yield locus from crystallographic data, two convex dual potentials will be used, from which the stress tensor can be derived as a function of the plastic strain rate tensor and vice versa, as shown in sections 2.1 and 2.2. This potential function is given by the rate of plastic work per unit

volume (equation (1)):

$$P=\phi(\underline{s})=\psi(\underline{\dot{e}}^P)=s_p\dot{e}^P_p, \quad (1)$$

where $\underline{s}$ and $\underline{\dot{e}}^P$ are the five-dimensional representation of the deviatoric stress tensor minus the back stress (see equation (7)) and the plastic strain rate respectively.

2.1 Texture-based strain rate space potential

Let $\dot{e}^P$ and $\underline{u}$ be respectively the magnitude and the direction of a plastic strain rate.

$$\underline{u}=\frac{\underline{\dot{e}}^P}{\dot{e}^P} \text{ with } \dot{e}^P=\sqrt{\dot{e}^P_p\dot{e}^P_p}. \quad (2)$$

By definition of rate insensitivity, the stress $\underline{s}$ corresponding to a given plastic strain rate $\underline{\dot{e}}^P$ does not depend on $\dot{e}^P$ but only on $\underline{u}$, so equation (1) can be rewritten as:

$$P=s_pu_p\dot{e}^P. \quad (3)$$

Van Houtte and al. [1989], proposed to use a dimensionless function of $\underline{u}$:

$$s_pu_p=\tau Q^{II}(\underline{u}), \quad (4)$$

where τ is the value of the critical resolved shear stress (CRSS) which is assumed to be the same on all the slip systems. The function Q^{II} represents the average Taylor factor and it is expressed as a polynomial series expansion defined in the strain rate space:

$$Q^{II}(\underline{u})=F_{p_1p_2\ldots p_N}u_{p_1}u_{p_2}\ldots u_{p_N}, \quad (5)$$

where the indices satisfy the condition $1\le p_1\le p_2\ldots\le p_N\le 5$. In equation (5), N is the order of the series expansion and is equal to 6 in this case. The coefficients of the series expansions can be calculated by a least square fitting on the average Taylor's factor directly computed using the texture measurement.

From equation (4), P can be written as:

$$P=\tau\dot{e}^PQ^{II}(\underline{u}). \quad (6)$$

Then, the gradient of the defined potential gives the deviatoric yield stress corresponding to any strain rate direction $\underline{u}$:

$$s_p=\hat{\sigma}_p-x_p=\tau\frac{\partial(\dot{e}^PQ^{II}(\underline{u}))}{\partial\dot{e}^P_p}, \quad (7)$$

where $\underline{x}$ represents the center of the yield locus, τ gives its size and the partial derivative as a function of $\underline{\dot{e}}^P$ corresponds to its shape.

2.2 Texture-based stress space potential

A unique yield locus in five-dimensional stress space can be represented by the following expression:

$$\tau=sQ^I(\underline{s}^*), \quad (8)$$

where $Q^I(\underline{s}^*)$ is a function of the stress direction $\underline{s}^*$ and s is the length of the radius vector such that $s\,\underline{s}^*$ lies on the yield surface.

To find the stress radii s for a set of stress directions $\underline{s}^*$, the following minimization procedure has to be done:

$$\frac{s}{\tau}=\min_{\underline{u}}\frac{Q^{II}(\underline{u})}{\underline{u}\,\underline{s}^*}. \quad (9)$$

The scale factor τ clearly shows that the shape does not depend on the size of the yield locus.

The series expansion for the function $Q^I(\underline{s}^*)$ can be written by analogy with equation (5) as:

$$Q^I(\underline{s}^*)=G_{p_1p_2\ldots p_N}s^*_{p_1}s^*_{p_2}\ldots s^*_{p_N}, \quad (10)$$

the coefficients $G_{p_1p_2\ldots p_N}$ of the series expansion are obtained by a least squares fitting to the inverse of the stress radii, i.e. to τ/s, for all the different stress modes $\underline{s}^*$ instead of the Taylor factors as in section 2.1.

The strain rate mode $\underline{u}$ corresponding to a stress mode $\underline{s}^*$ can be calculated by:

$$u_p=\lambda\frac{\partial(sQ^I(\underline{s}^*))}{\partial s_p}, \quad (11)$$

which is analogous to equation (7) except for the parameter λ that has to be chosen here, such that $\underline{u}$ has the unit length.

2.3 Hardening models

Two hardening models based on texture will be briefly described. The first one, TexIso (strain rate space formulation, Hoferlin [2001]), is an isotropic hardening where τ is assumed to be a function of the average polycrystal slip Γ:

$$\tau=k'\left(\Gamma+\Gamma_0\right)^{n'}, \tag{12}$$

a simple micro-macro link applied on an uniaxial tensile test allows to identify the k', Γ_0 and n'.

The second one, TexMic (strain rate space formulation, Hoferlin [2001]), is based on Teodosiu's hardening law (Teodosiu and Hu [1995]), and takes into account the evolution of dislocation substructures during reversed deformation. It explains the strain hardening stagnation and the influence of the amount of pre-stress. It allows to model the Bauschinger effect and strong path changes such as ones observed during complex loading modes. The complete set of internal variables is denoted by $\left(\underline{\underline{S}},\underline{P},\underline{\alpha},R\right)$. $\underline{\underline{S}}$, $\underline{\alpha}$ and R have the dimension of stress, $\underline{P}$ is dimensionless. For a well-annealed material, all their initial values are zero.

$\underline{\underline{S}}$ (fourth order tensor) describes the directional strength of an intragranular structure. $\underline{P}$ (second order tensor) indicates strain-path changes, it is associated with the polarity of the persistent dislocation structures and saturates toward the direction of strain rate tensor $\underline{N}_{\dot{\varepsilon}_p}$ (tensioral form of $\underline{u}$). $\underline{\alpha}$ (second order tensor and tensioral form of $\underline{x}$) describes the back stress and R takes into account the isotropic hardening by the statistically accumulated dislocations. If $\underline{\underline{S}}$ is decomposed as shown in equation (13) (where $\otimes$ is the cross-product) the evolution of these state variables is represented by equations (14) to (18) denoting by $^{\nabla}$ the Jaumann objective rate.

$$\underline{\underline{S}}=S_D\underline{N}_{\dot{\varepsilon}_p}\otimes\underline{N}_{\dot{\varepsilon}_p}+\underline{\underline{S}}_L \tag{13}$$

$$\dot{S}_D=C_S\left[g\left(S_{sat}-S_D\right)-hS_D\right]\dot{\Gamma} \tag{14}$$

$$\overset{\nabla}{\underline{\underline{S}}}_L=-C_{SL}\left(\frac{S_L}{S_{sat}}\right)^{nL}\underline{\underline{S}}_L\dot{\Gamma} \tag{15}$$

$$\overset{\nabla}{\underline{P}}=C_P\left(\underline{N}_{\dot{\varepsilon}_p}-\underline{P}\right)\dot{\Gamma} \tag{16}$$

$$\overset{\nabla}{\underline{\alpha}}=C_\alpha\left(\alpha_{sat}\underline{N}_{\dot{\varepsilon}_p}-\underline{\alpha}\right)\dot{\Gamma} \tag{17}$$

$$\dot{R}=C_R\left(R_{sat}-R\right)\dot{\Gamma} \tag{18}$$

Equations (19) to (24) complete the description of the model. τ_0, α_0, S_{sat}, R_{sat}, C_p, C_{SL}, C_{SD}, C_x, C_R, n_p, n_L, m, q are material parameters.

$$S_D=\underline{N}_{\dot{\varepsilon}_p}:\underline{\underline{S}}:\underline{N}_{\dot{\varepsilon}_p} \tag{19}$$

$$S_L=\left|\underline{\underline{S}}_L\right| \tag{20}$$

$$P_D=\underline{P}:\underline{N}_{\dot{\varepsilon}_p} \tag{21}$$

$$\alpha_{sat}=\alpha_0+\left(1-m\right)\sqrt{S_D^2+qS_L^2} \tag{22}$$

$$h=\frac{1}{2}\left(1-\frac{\underline{\alpha}:\underline{N}_{\dot{\varepsilon}_p}}{\alpha_{sat}Q}\right) \tag{23}$$

$$g=\begin{cases}1-\dfrac{C_P}{C_{SD}+C_P}\left|\dfrac{S_D}{S_{sat}}-P_D\right| & \text{if } P_D\geq 0\\ \left(1+P_D\right)^{n_P}\left(1-\dfrac{C_PS_D}{C_{SD}+C_PS_{sat}}\right) & \text{if } P_D<0\end{cases} \tag{24}$$

The final hardening model is defined by:

$$\tau=\tau_0+m\left|\underline{\underline{S}}\right|+R\,. \tag{25}$$

3. FINITE ELEMENT FORMULATION

3.1 Solid element BLZ3D

It is a mixed type element with eight nodes and one integration point (Zhu and Cescotto, [1994]). It is based on the Hu-Washizu principle, which is formulated on three fields: displacement, strain and stress. Special cares such as anti-hourglass stresses and assumed strain method are taken to avoid spurious zero-energy modes and incompressibility locking.

3.2 Contact element CFI3D

It is simulated by an interface element based on a penalty approach and derived from de virtual work

principle (Habraken and Cescotto [1998]). Kinetically compatible with the associated solid element, this element is defined by an isoparametrical approach and its numerical integration is carried out by Gaussian points. The originality of the present approach lies in the fact that the contact conditions (Signorini's condition and Coulomb friction law) are expressed at some integration points, not at nodal points.

3.3 Additive hypo-elastic formulation

As the anisotropic yield locii is defined according to material principal axes, some local reference system must follow these material axes during the large strains and rotations of the sheet. Real material axes attached to a deforming body are subjected to distortion, while local axes remain Cartesian. So, there is no unique definition of a local frame, however the various possible choices differ only through a spurious rigid body rotation. In Lagamine code, the method implemented to follow material axes is due to Munhoven and details can be found in Munhoven [1995] or Munhoven and al. [1995]. Working in hypo-elastic formulation, constitutive equations are not required for a plastic spin. This choice of hypo-elastic formulation has different advantages and remains physically sound as long as the elastic strains are small. A discussion on this choice can be found in Hoferlin [2001] .

4. APPLICATION

The geometry of the simulated deep-drawing process is the following one: a 100 mm long punch with a diameter of 150 mm and a curvature radius of 10 mm, a die with a curvature radius of 10 mm and a blank holder are the drawing tools. The drawing ratio is 2.0; the blank holder force is 98.1 kN; the simulation is performed up to a drawing depth of 80 mm. The blank is a 0.8 mm thick high strength steel sheet.

As we focus on the texture, the shape of the yield locus is deduced from the Orientation Distribution Function (ODF), which has been measured by X-ray diffraction.

The numerical data for this steel are obtained from a simple tensile test for the TexIso hardening behavior: k'=173.59, Γ_0=0.007827, n'=0.1726. The parameters for TexMic hardening law are τ_0=60 MPa, α_0=20 MPa, S_{sat}=83.03 MPa, R_{sat}=27.86 MPa, C_p=2.66, C_{SL}=4.76, C_{SD}=1.89, C_x=100, C_R=9.55, n_p=27.1, n_L=1.87, m=0.6, q=3.9. These parameters are not fully representative of the studied steel as only τ_0, α_0, C_p were identified thanks to the available tensile tests. The other parameters are typical ones for a deep drawing steel (Hoferlin [2001]). The Young's modulus is 209880 MPa and the Poisson ratio is 0.28.

Due to the orthotropy of the problem only one quarter is modeled (see Figure 1), using for the blank a three-layer mesh made up of 2256 BLZ3D elements. The die, punch and blank holder are modeled by 1085 triangular foundation elements and the contact between the blank and the tools by 2257 CFI3D contact elements.

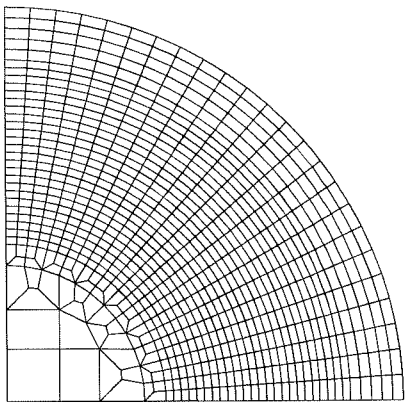

Figure 1. Initial configuration.

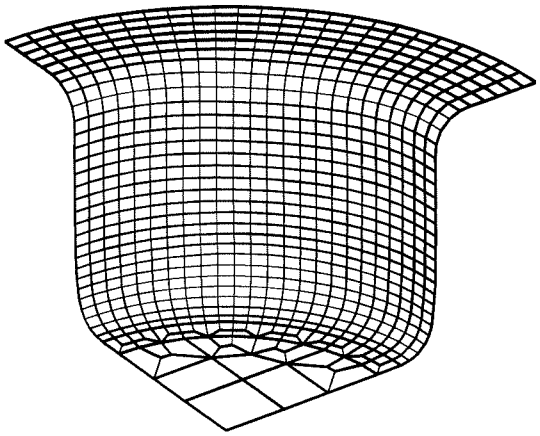

Figure 2. Final shape of the mesh.

Three simulations were done using the TexIso, TexMic and ANI3VH (stress space formulation with an isotropic hardening law, Winters [1996]) constitutive laws. Figure 2 shows the final shape of the mesh for the simulation with TexIso constitutive law. The results are compared with experimental measures. Figure 3 shows the deep-drawing force with respect to the cup's depth. It can be seen that constitutive laws TexIso and ANI3VH, which use the same isotropic hardening law, provide curves of identical shape but with a stiffer behavior for ANI3VH. This difference could be explained by the supplementary minimization required to calculated the yield locus or due to the effect of the different integration schemes used. The shape of the TexMic curve is the one which agrees the best with the experimental curve. It appears to be stiffer than TexIso, in spite of their same formulation in strain rate space. This difference can only be related to the hardening behavior which modifies the yield locus size and location.

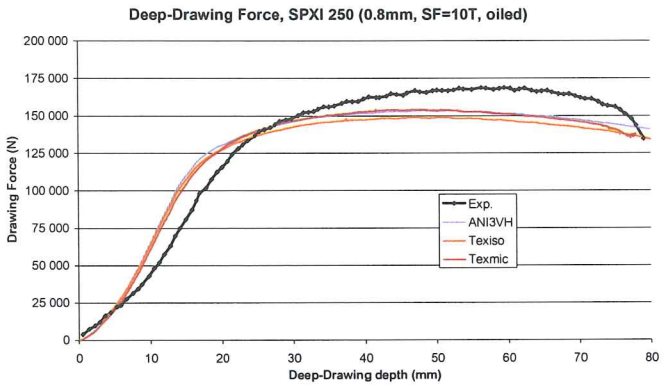

Figure 3. Deep-drawing force.

The plane principal strains E_1, E_2, and the thickness strain E_3 at 0°, 45° and 90° with respect to the rolling direction (RD) are analyzed in Figures 4, 5, 6, in which three zones are identified: zone I, zone II and zone III according to curvilinear abscises from the center. Zone I is defined for abscises smaller than 80 mm and represents the sheet part under the punch, zone II from 80 mm to 140 mm consists in the wall cup and zone III represents the sheet still under the blank-holder. In zone I (small strain zone) TexMic results are the closest to the experimental curve. Strains obtained by these three constitutive models show the same tendency in the next two zones, but in zone II TexMic has the best accuracy in most of the cases. TexIso and ANI3VH fit better in zone III. Picks observed in transition zones could be related to numerical perturbation due to a too coarse discretization. This point has to be investigated.

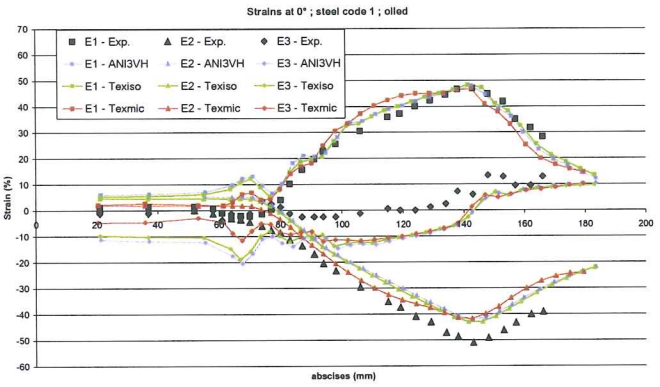

Figure 4. Strains at 0° with respect the RD.

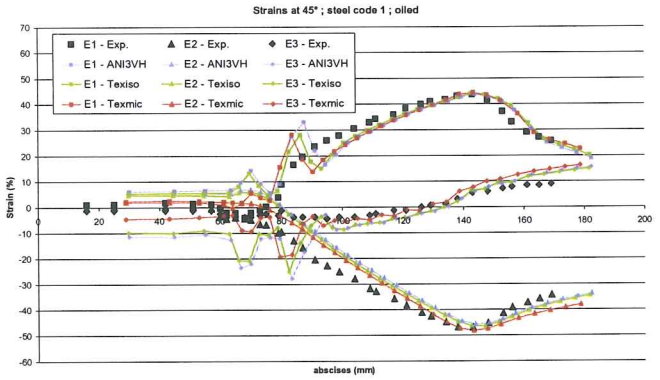

Figure 5. Strains at 45° with respect the RD.

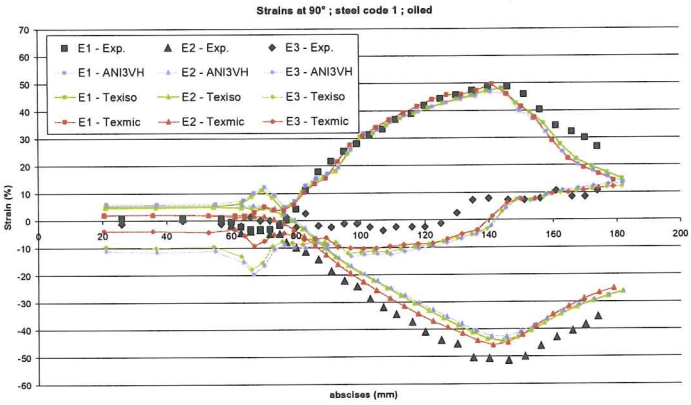

Figure 6. Strains at 90° with respect the RD.

Earing behavior is depicted in Figure 7, showing that the closest level is achieved by TexMic, but no model is able to represent the correct shape.

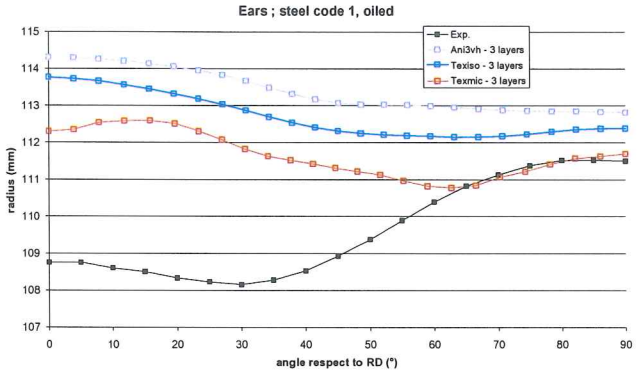

Figure 7. Earing behavior.

5. CONCLUSIONS

The behavior of three constitutive models is presented. The deformation analysis suggests that TexMic better represents the beginning of the plastic flow, i.e. small strain zone, but also the punch force curve at the end of the drawing process. This shows the interest of a hardening law closer to the microscopic events of the material. The earing profile, different from the simulated one, is still not clearly explained. Simulations with texture evolution do not bring any answer. Other factors such as the stiffness of BLZ3D element or contact penalty approach are currently studied as well as the earing profiles of another steel.

ACKNOWLEDGEMENTS

The authors gratefully acknowledge Professors P. Van Houtte and C. Teodosiu who allow the use of TexMic law. We are deeply grateful to Dr. E. Hoferlin for his technical guidance with the implementation of this law in our *Lagamine* version.

As Research Associate of National Fund for Scientific Research (Belgium), A. M. Habraken thanks this Belgian research fund for its support.

REFERENCES

[1] A. Van Bael, 1994, Anisotropic yield loci derived from crystallographic data and their application in finite-element simulations of plastic forming processes, Ph.D. Thesis, Katholieke Universiteit Leuven.

[2] J. Winters, 1996, Implementation of a texture-based yield locus into an elastoplastic finite element code. Application to sheet forming, Ph.D Thesis, Katholieke Universiteit Leuven.

[3] E. Hoferlin, 2001, Incorporation of an accurate model of texture and strain-path induced anisotropy in simulations of sheet metal forming, Ph.D Thesis, Katholieke Universiteit Leuven.

[4] C. Teodosiu and Z. Hu, 1995, Evolution of the intragranular microstructure at moderate and large strains: Modeling and computational significance, Simulation of Materials Processing: Theory, Methods and Applications, Proceedings of Numiform '95, eds. S. Shen & P.R. Dawson, 173-182. Balkema, Rotterdam.

[5] P. Van Houtte, K. Mols, A. Van Bael, E. Aernoudt, 1989, Application of yield loci calculated from texture data, Textures and Microstructures, vol. 11, 23-39.

[6] Y.Y. Zhu and S. Cescotto, 1994, Transient thermal and thermomechanical analysis by F.E.M., Computers and Structures, 53(2), 275-304.

[7] A.M. Habraken, S. Cescotto, 1994, Contact between deformable solids, the fully coupled approach, Mathematical and Computer Modelling, 28(4-8), 153-169.

[8] S. Munhoven, 1995, Velocity gradients and local axes in three-dimensional finite element simulations, M.S.M. Internal Report N°219, Université de Liège.

[9] S. Munhoven, A.M. Habraken, J. Winters, R. Schouwenaars, P. Van Houtte, 1995, Application of an anisotropic yield locus based on texture to a deep drawing simulation, NUMIFORM 95 Simulation of materials Processing: Theory, Methods and Applications, Shen&Dawson editors, Balkema, 767-772.